A review on hierarchical porous carbon derived from various 3D printing techniques

Journal:	*Nanoscale*
Manuscript ID	NR-REV-01-2024-000401.R1
Article Type:	Review Article
Date Submitted by the Author:	16-Apr-2024
Complete List of Authors:	Romero, Cameron ; University of Louisiana at Lafayette, Chemical Engineering Liu, Zhi; University of Louisiana at Lafayette, Chemical Engineering Wei, Zhen; University of Louisiana at Lafayette, Chemical Engineering Fei, Ling; University of Louisiana at Lafayette, Chemical Engineering

SCHOLARONE™
Manuscripts

ARTICLE

A review on hierarchical porous carbon derived from various 3D printing techniques

Cameron Romero[†], Zhi Liu[†], Zhen Wei, and Ling Fei[*]

Hierarchical porous carbon is an area of advanced materials that play a pivotal role in meeting the increasing demands across various industry sectors including catalysis, adsorption, energy storage and conversion. Additive manufacturing is a promising technique to synthesize architectured porous carbon with exceptional design flexibility, guided by computer-aided precision. This review paper aims to provide an overview of porous carbon derived from various additive manufacturing techniques, including material extrusion, vat polymerization, and powder bed fusion. The respective advantages and limitations of these techniques will be examined. Some exemplary work for various applications will be showcased. Furthermore, perspectives on future research directions, opportunities, and challenges of additive manufacturing for porous carbon will also be offered.

1. Introduction

Porous carbon materials have emerged as promising candidates in sectors such as water purification,[1] gas adsorption/separation,[2] catalyst supports,[3] energy storage and conversion amongst many others.[4–6] This prominence is due to its many distinct properties and advantages, setting it apart from other materials. Firstly, it has a high specific surface area that can increase the number of active sites present, fostering an improved interaction with targeted molecules. Additionally, the pores in the material can be tailored, encompassing aspects such as pore size distribution and volume, which increases its performance for specific applications.[7–9] In general, these porous carbon materials are categorized based on their pore size with the smallest being microporous (pore size < 2 nm), followed by mesoporous (2 nm ≤ pore size ≤ 50 nm), and finally macroporous (pore size > 50 nm).[10] Additionally, certain types of carbons exhibit excellent electrical conductivity, rendering them applicable in areas like energy conversion and storage.[11] Lastly, porous carbons' exceptional chemical stability ensures resilience against degradation/corrosion in severe environments, providing reliability in a wide array of applications.[12]

One of the most common approaches to synthesizing porous carbon is physical activation, where carbon precursors are heated in the presence of activating agents such as steam or

CO_2, forming pores within the carbon structure.[13] Chemical activation is another method which employs agents like KOH that interact with precursors to create controlled pores during heating.[14] The primary difference in chemical and physical activation is that in chemical, the precursor is impregnated with the agent and then heated as opposed to the agent simply being in the presence of the precursor. Additionally, pyrolysis of porous precursors has been widely used to produce porous carbon, including metal–organic frameworks (MOFs), at high temperatures to produce well-controlled, unique, porous structures. Alternatively, materials like porous SiO_2 can be used as a template, impregnating the carbon precursor and pyrolyzed, subsequently removing SiO_2 to leave behind a porous carbon framework.[15] Moreover, natural materials like wood possess a unique heterogeneous biostructure, contributing significantly to the microstructure development during synthesis steps. These materials also serve as excellent renewable sources for porous carbon.[16] Most of the synthesis methodologies mentioned above generally result in powdered forms of porous carbon. While these methods allow precise control at the microscopic level for individual carbon particles, they often provide limited control over the macroscopic architecture of the entire material, such as electrodes, when it comes to practical applications.

Macroscopic architecture has been proven equally crucial for optimizing performance.[17,18] Take supercapacitors as an example, where porous carbon is extensively employed. The synthesized powder must be transformed into electrodes. Presently, the slurry coating method lacks precise control over the macroscopic architecture of the electrodes.[19,20] Specifically, porous carbon particles are distributed randomly on a statistical basis. Achieving control at both the individual particle level (micro/meso pores) and the macroscopic structure of the final electrodes would represent a significant advancement.

Department of Chemical Engineering, University of Louisiana at Lafayette
Correspondence: ling.fei@louisiana.edu
† Authors contributed to the manuscript equally

Three-dimensional (3D) printing, also known as additive manufacturing, offers an efficient, cost-effective, and consistent approach to creating architectured porous carbon by simplifying the production procedure to layered manufacturing.[21] This class of techniques can provide precise control over the thickness, porosity, rigidity, and geometrical shape of the material from both a microscopic and macroscopic point of reference.[22] To date, numerous excellent review articles are available on the synthesis of porous carbon in powder forms, covering various carbon classifications and applications.[23–27] Additionally, review articles concentrating on the advancements in 3D printing are also available.[28–32] Notably, Blyweert et al. reviewed advances in 3D carbon printing and provided insight into the functional carbon-based systems. It discusses carbon systems in general rather than with the sole focus on porous carbon. Thereby, this work serves as a complementary resource to the unique properties and opportunities of porous carbon materials by 3D printing, which is critical for further advancing their practical applications in various fields.[33] With this in mind, there is a lack of review on porous carbon derived from various 3D printing techniques. The related statistics of publications over the past few decades collected from Web of Science by inputting keywords of "3D printing" and "porous carbon" are presented in Figure 1a, showcasing the escalating trend in studies on 3D printing technology and its combination with porous carbon materials. Therefore, it would be greatly beneficial to have such a summary and discussion on porous carbon derived from diverse 3D printing techniques. This review aims to bridge this gap by initially offering an overview of advanced 3D printing methods. Then, it is followed by a brief showcase and discussion of exemplary porous carbon prepared by each printing method. Finally, some perspectives and directions on advancements in 3D printing to produce porous carbon will be shared. It's important to note that we distinguish between a void and a pore for simplification in this review. To be clear, a void represents an empty space within a computer-designed structure, while a pore indicates an opening within the material itself, which is all summarized in Figure 1b.

2. 3D printing overview

A variety of 3D printing techniques have been developed to cater to specific applications. In 2015, the American Society of Testing and Materials (ASTM) catalogued 3D printing technologies into seven main groups based on technical features: Material Extrusion, Vat Polymerization, Powder Bed Fusion, Material Jetting, Binder Jetting, Direct Energy Deposition and Sheet Lamination.[34] One of the technical features analyzed was the material used. Since the creation of porous carbon requires carbon precursors, only the techniques that utilized plastics/resins will be analyzed. As a result, this section provides an overview and comparison of Material Extrusion, Vat Polymerization, and Powder Bed Fusion with the aim of discussing operational principles, advantages, limitations,

and suitability. All the information listed within this section is summarized in Table 1.[35–43]

2.1 Material Extrusion

Material extrusion, often referred to as Fused Deposition Modeling (FDM), is a 3D printing method that uses ink or filament fed through a heated nozzle. The filament is heated to just above its melting point, creating a molten material that is deposited onto a print bed by moving the nozzle along the x, y, and z axes to form the desired object. Once deposited, the material rapidly solidified to create a strong and durable final product. This basic working principles of material extrusion can be seen in Figure 2.[44]

One of the main advantages of material extrusion lies in its adaptability to a wide range of materials.[45] Researchers can select from a diverse array of thermoplastic filaments, each with unique properties and characteristics. This allows for the creation of components with tailored attributes, making it a versatile tool in various industries.[46] Moreover, the presence of various nozzle diameters and layer thicknesses provides further flexibility in the design and fabrication process.[47] This allows the user to fine-tune their builds to precise specifications. Alongside its material adaptability, material extrusion excels in cost-effectiveness as FDM printers are notably more budget friendly, expanding accessibility to a wider spectrum of researchers and institutions. Lastly, the straightforwardness of the process streamlines operation and upkeep, making it an accessible choice for projects of varying sizes and complexities.[48]

While material extrusion offers significant advantages, it does come with its set of limitations. Most notably, the process is less suitable for producing intricate parts due to the circular profile of the print nozzle, resulting in layer thickness equal to the diameter of the nozzle. These visible layers often result in a stair-stepped effect and require post processing to achieve a smooth surface, which takes time and can get messy.[49] Furthermore, the bond and strength of the printed part are usually weakest along the plane of the layer interface, resulting in compromised rigidity. Moreover, since the printed builds are coming out of the tip of the nozzle, any scale up will take more time in a linear fashion.[50] Finally, certain filaments may experience degradation or undesirable phase transitions during the high-temperature printing process, necessitating careful consideration of the printing parameters for successful outcomes.[51]

2.2 Vat Polymerization

Vat polymerization is a family of 3D printing techniques that uses a build platform, ultraviolet light, and a vat of photopolymer resin to create three-dimensional objects. The build platform is submerged in the resin and the light is shined in a pre-coded manner to cure the resin layer-by-layer. As each layer is solidified, the build platform is moved further from the light source (typically in intervals between 10 and 50 µm) to allow more resin to infill and cure. The light source can be applied to either the bottom or top of the printer and is dictated

by the resin's fluid properties. A schematic of both orientations of the layer-based vat photopolymerization printing process can be seen in Figure 3.[52]

The most attractive feature of vat polymerization printing is the use of ultraviolet light that allows for the creation of intricate, highly detailed parts with an extreme level of accuracy and resolution.[53] Consequently, the cured resin tends to exhibit smooth surface finishes, thereby reducing the need for extensive post-processing steps.[54] Additionally, this method offers a broad spectrum of material options, encompassing specialized resins with varying properties such as flexibility, transparency, and biocompatibility. The remarkable versatility in material selection highlights the adaptability to cater to specific research or application needs, facilitating the creation of components with a wide range of properties, spanning from rigid and durable to flexible and elastomeric.[55] Lastly, upscaling does not add additional time since the print duration is solely a function of the height of the build(s), rather than the volume consumed.[56]

The drawback of vat polymerization is the restrictions on build size. Both the size of the 3D printer as well as the volume of resin vat impose constraints on the maximum dimensions of the printed object, limiting its suitability for large-scale prints.[57] Additionally, the process can be sensitive to ambient conditions, particularly temperature, humidity, and luminosity, which can influence the curing process and affect the final print quality.[58] Another factor to consider is the cost associated with specialized photopolymer resins, which can be relatively expensive.[59] Finally, due to the intricate detailing and the build platform moving along the gravity axis, supports are often required to prevent the object from deforming.[56]

2.3 Powder Bed Fusion

Powder bed fusion is a printing method that uses an energy source (e.g., thermal energy, laser) to selectively melt and fuse together fine powder particles. It is composed of two main compartments: a powder reservoir and a build platform. To begin, the reservoir is filled with round and smooth powder that is heated to just under its melting point. A powder spreader, usually a roller or blade, is then used to distribute a thin, uniform layer of powder on the build plate. A high-powered laser then selectively heats up regions of the powder, fusing together the particles. The build platform is then lowered while the powder reservoir is raised, and the process is repeated until the final product is created. A schematic of powder bed fusion can be found in Figure 4.[60]

One of the biggest advantages of powder bed fusion compared to other 3D printing techniques lies in its ability to produce complex, fully functional internal structures with fine details. This is achieved by utilizing unfused powder as a support, granting an unprecedented level of geometric freedom. Unlike traditional methods, not every part of the component needs to be connected during the printing process, allowing for unparalleled design complexity and functionality.[61] Additionally, the printing method allows for tight adhesion between its layers with minimal waste. Furthermore, scale up is viable since the

most time-consuming step is spreading a new layer of powder.[60,62]

While powder bed fusion boasts impressive advantages, it is important to consider some of its drawbacks. For starters, the equipment is relatively expensive, making it less accessible.[63] Additionally, the post-processing stage presents its own set of complexities. Each printed part must be carefully extracted from the powder bed and thoroughly cleaned; a task that becomes more intricate and time-consuming as the size of the print gets smaller. There are integrated powder removing systems that can de-powder parts and recycle unused powder, but these systems are expensive and are still in the developmental phase.[64] Finally, the use of high-powered lasers in the process demands strict adherence to safety protocols to mitigate any potential hazards.[65]

3. Porous Carbon from 3D printing

Each category of 3D printing has subcategories with unique advantages, limitations, and applications tailored to a targeted process. As demand for 3D printing continues to grow, these subcategories are constantly being developed and refined. While the previous section provided an overview of the general mechanisms and pros and cons of each additive manufacturing technique that utilizes plastics/resins, the next section will focus specifically on the subcategories that have been used to create porous carbon.

3.1 Porous Carbon Derived from Material Extrusion

The most common material extrusion method that utilizes carbon-based ink is direct ink writing, more commonly referred to as DIW. The ink for this method is typically composed of functional fillers, binders, solvents, and additives.[66] In regard to porous carbon, the functional filler would be a carbon precursor, which would change depending on the intended purpose. The binders help to uniformly disperse the ink within the syringe. The binder must be compatible with the functional filler, provide good adhesion, and, in most cases, allow for easy removal after printing to increase the density of functional fillers. The solvent is used to modify the viscosity to affect the dispensation and drying rate. Finally, additives can be implemented to enhance the final characteristics.[67]

The versatility of components within the DIW printing method makes it attractive for many applications. For instance, Liu et al. were able to manufacture a monolithic nitrogen-doped porous carbon material via DIW method for the removal of methylene blue (MB). The ink consisted of starch and gelatin as the carbon source, melamine as the nitrogen additive, water as the solvent, and silicon dioxide as the filler and template. The mixture was printed, carbonized, and then treated with NaOH and HNO_3 to produce the meso/macro nitrogen-doped porous carbon (Figure 5), which allowed for the easy adsorption of MB without the need for centrifugation, filtration, or magnetic separation. The microscopic pore structure size and specific surface area of the material could be controlled by adjusting the size of the SiO_2 templates.[68] The results proved that the DIW printed porous

carbon materials are promising in the realm of adsorption and catalysis.

More recently, Zhou et al. utilized the DIW method to print a catalyst for the oxidation of benzyl alcohol. To do this, SiO_2 spheres with different diameters were prepared via the Stöber method. The ink was a mixture of starch, gelatin, and the SiO_2 spheres. After printing, carbonization, and treatment with NaOH and HNO_3, they found that the smaller SiO_2 spheres led to better oxidation of the benzyl alcohol due to the increased surface area of the porous carbon (Figure 6). This simple, low cost, and reliable method proved to hold great promise for further catalytic applications.[69]

In other works, Yang et al. prepared a 3D nitrogen-doped porous carbon aerogel by DIW printing and subsequent freeze-drying and pyrolysis. The ink consisted of agarose, urea, sodium chloride, and hydroxypropyl methylcellulose (Figure 7). The obtained structure exhibited multiple desirable properties, including self-supportability, hierarchical porous structure, and good structural stability, allowing for use in home-built water flow-through devices for continuous treatment of *Escherichia coli* (*E. coil*) culture. It led to 100% inactivation of bacteria for at least 5 hours, which far exceeds the capabilities of traditional catalysts.[70]

Yao et al.[71] fabricated a 3D-printed multiscale porous carbon aerogel (3D-MCA) using a unique blend of chemical methods and the direct ink writing technique. Micropores significantly increase the electrode's specific surface area, while the macro- and mesopores serve as electrolyte reservoirs, drastically shortening the ion diffusion length during rapid charging. The 3D-MCA boasts an open porous structure and an impressive surface area of approximately 1750 m^2 g^{-1}. Remarkably, the symmetric device achieves a stunning capacitance of 148.6 F g^{-1} at a rate of 5 mV s^{-1}, even at the chilling temperature of −70 °C. Moreover, it retains an impressive capacitance of 71.4 F g^{-1} at an accelerated scan rate of 200 mV s^{-1}, which is 6.5 times higher than that of its non-3D printed MCA counterpart. These outstanding results rank among the top performances reported for low temperature supercapacitors, highlighting the critical role of open porous structures in sustaining capacitive performance at ultralow temperatures.

Li et al.[72] proposed a reduced graphene oxide (rGO)/Super-P aerogel composite electrode with a controllable porous structure, leveraging the innovative technique of direct ink writing (DIW). The DIW technique allows for precise control over both the macroscale and microscale porous structure of graphene aerogel. This control is facilitated by varying the printing path and the concentration of GO. The meticulously designed porous architecture provides an increased specific surface area for reaction, reduces the mass transfer path, and enhances ion accessibility. These attributes contribute to a decrease in electrochemical polarization and an improvement in reactive ions accessibility. Moreover, the 3D printed graphene aerogel boasts advantages such as low density, high porosity, superior mechanical properties, large specific surface area, and unique electrochemical properties. The cell equipped with the optimized rGO/Super-P aerogel electrode demonstrates a superior discharge capacity of 848.4 mA h at a current density of 80 mA cm^{-2}. This performance represents a noteworthy 14.9% enhancement compared to a cell equipped with the traditional graphite felt (GF), underscoring the potential of a 3D printing approach in VRFB applications.

Aerosol jet printing (AJP), a novel non-contact direct writing technique, is specifically designed to achieve precise and intricate patterns on a variety of substrates.[73] Parate et al.[74] reported on an innovative aerosol-jet-printed (AJP) graphene-based immunosensor, which is capable of monitoring two distinct cytokines: interferon gamma (IFN-γ) and interleukin 10 (IL-10). To create this sophisticated device, interdigitated electrodes (IDEs) were printed with a 40 μm finger width using graphene-nitrocellulose ink on a durable polyimide substrate. The IDEs were then subjected to an annealing process in CO2, a critical step that introduces reactive oxygen species onto the graphene surface. These oxygen species function as chemical handles, providing bonding sites to covalently attach IFN-γ and IL-10 antibodies to the graphene surfaces, thereby enhancing sensitivity. The resultant AJP electrochemical immunosensors exhibit a wide sensing range (IFN-γ: 0.1–5 ng/mL; IL-10: 0.1–2 ng/mL), a remarkably low detection limit (IFN-γ: 25 pg/ml and IL-10: 46 pg/ml), and, most importantly, high selectivity, with the antibodies demonstrating minimal cross-reactivity with each other or IL-6.

In general, the process of utilizing material extrusion to create porous carbon has been popularly applied to catalytic, adsorption, and absorption processes. This is because these processes primarily rely on the surface properties of the printed material, not their geometries. As a result, the simplicity and cost-effectiveness of material extrusion, along with its ability to generate porous carbon structures, makes it an invaluable tool in these applications despite low-resolution prints. Ongoing research and development in this field continue to address its limitations (layer-layer interface weakness,[75] post-processing requirements,[76] limited resolution,[77] and limits on high-temperature materials[78]). Solutions to these issues will expand material extrusion's potential applications and increase its effectiveness.

3.2 Porous Carbon Derived from Vat Polymerization

Stereolithography (SLA) is a promising vat polymerization technique for creating porous carbon. The resin is composed of photoinitiators, liquid monomers, and oligomers. These components are cross-linked in a layer-by-layer fashion by selectively photopolymerizing portions of the resin by means of a rastering laser. This method results in a high resolution (≥10 μm), making it possible to derive porous carbon structures with intricate details.[52]

Steldinger et al. obtained hierarchical structured porous carbons from stereolithography and copolymerization of pentaerythritol tetraacrylate and divinylbenzene. The photocurable resin (35% pentaerythitol tetraacrylate, 35% divinylbenzene, and 30% bis(2-ethylhexyl) phthalate) was printed and treated to create carbon with superb mechanical strength as well as a high surface area (2200 m^2 g^{-1}) through activation.[79] The entire process can be seen in Figure 8. This

study showed the ability for SLA to combine fast printing to produce porous carbon with high mechanical strength, making it excellent for porous carbon applications that require a robust nature.

Wang et al. developed a novel hybrid manufacturing method to fabricate 3D hierarchical porous carbon electrodes for electrochemical energy storage. The approach utilized SLA 3D printing with KOH chemical activation to create macro, meso, and microporous carbon (Figure 9). In order to tune the pore size, different ratios of KOH to carbon material were employed and studied, which showed that an increase in KOH will decrease the pore size and result in better electrochemical results. This correlation is ascribed to the fact that an ideal porous carbon electrode must allow for fast mass diffusion routes for the ions as well as provide rapid electron transfer pathways.[80] Since SLA 3D printing not only produces porous carbon but does so in a controllable way for architectured electrode design with a high resolution, this makes it highly applicable in electrochemical energy storage and conversion applications, particularly when a complex electrode structure is required.

Blyweert et al. demonstrated for the first time an effective strategy to develop 3D-printed carbon material from bio-based resins using stereolithography.[33] Traditional resins are made based on petrochemical origins, which often have a low carbon yield and undergo significant volume shrinkage (50-90%) after pyrolysis. To address this, the group added condensed tannin (a wood extract) to the resin, printed, post-cured, and pyrolyzed the component to produce a porous carbon lattice. The results yielded about 20% carbon content with a reduced warpage and volume shrinkage of approximately 35%, a significant increase to traditional neat resins. This work shows the potential of obtaining a sustainable, highly porous carbon build with complex architectures.

Jiang et al. fabricated a novel porous carbon model embedded with bismuth-based particles by SLA method and following calcination in air at low temperature, as the light-enhanced removal agent of chloride (Cl^-) in wastewater.[81] The preparation conditions were optimized to obtain a BET surface area of 40 m^2 g^{-1} with a more robust structure. The increase in structure strength was primarily due to the optimization of calcination temperature, which ensures sufficient carbonization while still maintaining the model's shape. The porous structure allows more active materials to adhere on the surface and achieves better performance on the removal of Cl^-. The resulting removal efficiency reached 26% in the acidic and dark conditions, whereas it can be largely improved to 63.6% by irradiation of UV light. It is notable that this Bi-based porous carbon model can be regenerated by treatment of NaOH after every removal cycle and reused for the next cycle, which efficiently reduces the cost of materials and benefits sustainability. This work provides a promising way to alleviate the pollution of Cl^- in the water and expands the application field of SLA technology.

More recently, Katsuyama et al. were able to utilize SLA combined with CO_2 gas activation to fabricate controlled macro and nano-porous carbon lattices for use as electrodes in supercapacitors.[82] The schematic of the whole synthetic route

is clearly shown in Figure 10. They then deposited MnO_2 onto the surface, which further enhanced the capacitance by a factor of 2.5 times. The achieved values are better than materials prepared by almost all other manufacturing methods to date in terms of areal energy and power densities. The findings confirm that maintaining macrostructure while simultaneously keeping an ordered microstructure can dramatically increase the power and energy output of a system owing to its ability to facilitate ion/electron transport within the material.

Building on these findings, Kudo et al. coupled SLA with hard template technique to achieve a hierarchical porous carbon microlattice with mechanical robustness and high surface area with mitigated volume shrinkage (Figure 11).[83] The work developed a composite photoresin consisting of magnesium oxide nanoparticles as a porogen template blended with graphene nanosheets to reduce UV scattering and contribute to the formation of micro/macropores. The printed material had a considerable compressive strength and Young's Modulus with gravimetric capacitance upwards of 105 F g^{-1}. This study shows that customizing the resin can allow for additives to be added prior to printing, highlighting that the prints can have a uniquely integrated structure with improved functional properties.

Heijden et al.[84] employed stereolithography 3D printing to manufacture model grid structures, which were then subjected to carbonization and evaluated as flow battery electrode materials. Porous electrodes play a crucial role in governing the electrochemical performance and pumping requirements in RFBs. However, conventional porous electrodes (e.g., carbon fiber based) have not been optimized to meet the specific requirements of liquid-phase electrochemistry. It is observed that the printing direction influences the electrode performance through a change in morphology, with diagonally printed electrodes exhibiting enhanced performance. Furthermore, mass transfer rates within the electrode are improved by helical or triangular pillar shapes, or by using interdigitated flow field designs. This study showcases the potential of stereolithography 3D printing to fabricate customized electrode scaffolds. This technology could facilitate the development of multiscale structures with superior electrochemical performance and reduced pumping losses, offering new avenues for electrode optimization in RFBs.

Chandrasekaran et al.[85] employed two advanced 3D printing methods - projection micro-stereo-lithography (PμSL) and two-photon polymerization direct laser writing (2PP-DLW) - to fabricate 3D sacrificial polymeric templates. These templates can range in size from millimeter to centimeter scale and feature intricate designs with details as small as tens of microns (PμSL) or even as minuscule as 100s of nanometers (2PP-DLW). The fabrication process of templated carbon aerogels (t-CAs) involves infiltrating the 3D-printed templates with resorcinol-formaldehyde (RF) precursor solution, followed by a high-temperature carbonization process at 1050 °C. During this stage, the RF precursor solution is converted into a CA while the 3D-printed template is simultaneously decomposed, leaving behind an intricate templated macroporous network structure. The presence of this templated macroporous architecture enhances mass transport within the t-CAs in comparison to traditional

bulk CA. This improvement is clearly demonstrated through more uniform activation and the t-CAs' superior response in electrochemical cyclic voltammetry and galvanostatic charge-discharge tests.

Employing vat polymerization technology for the fabrication of porous carbon materials marks a significant stride towards material science and engineering. The precision and versatility offered by vat polymerization enables the creation of intricate and customizable porous structures with accuracy and reproducibility, making it useful for various applications such as energy storage where architectured electrodes are desired.[86] Since UV light is the primary driving force to solidify the photocurable resin, additives can be implemented without thermal degradation, thus enhancing the feasibility of composite materials.[87] However, the amount of additive that can be added to the resin to form a composite is constrained. This limitation arises as the additive particles start to scatter or absorb UV light, thereby restricting the crosslinking process. As for the future of vat polymerization, improvements in resin chemistry,[88] UV laser characteristics, and printing parameters[56] will result in higher resolution prints, making its applications even broader, enhancing its effectiveness, and increasing the percent of additives within the resin.

3.3 Porous Carbon Derived from Powder Bed Fusion

Selective laser sintering (SLS), one of the oldest additive manufacturing techniques, is the most promising class of powder bed fusion to create porous carbon.[89] This process involves fusing carbon-rich precursors by heating a stock to a temperature directly lower than its melting point. Then, a rapid laser scans the surface, momentarily melting the precursor. The precursor immediately cools once the laser ceases, fusing the particles together in a stacking mechanism.[90] This being said, not all materials are suitable for SLS. The material must be in powder form, have the ability to sinter under the influence of a laser, and the powder needs to have a consistent particle size. With this, limited porous carbon has been derived from SLS in previous reports. However, since the process does not employ the use of binders or solvents, the end product has a high proportion of porous carbon.[91]

Guo et al. were able to fabricate porous carbon electrode precursors prepared using SLS 3D printing technology. These electrodes were then pyrolyzed through high temperature pyrolysis to create a mesoporous carbon material (Figure 12). One of the most attractive aspects of this synthesis is the use of pinewood powder as the carbon content, which allows for the recycling of agricultural and wood industry waste, reducing environmental pollution and saving material costs. The study looked at 30%, 40%, and 50% carbon content in the printed matrix, and found that as the percentage of carbon content increased, the internal tissues became loose, which lowered the effective conductive pathways.[92] Nevertheless, this study demonstrated that porous carbon can be derived from SLS 3D printing and done so in a sustainable, waste-reducing method that results in highly porous carbon.

Hong et al. successfully derived a two-step approach to create a carbon black/polyamide 12 composite material based on SLS technology. The first step involved adsorbing the carbon black onto the surface of polyamide 12 powders through ultrasonic and liquid phase-assisted absorption and deposition process. The composite parts were then sintered in the subsequent SLS process, which is entirely described in Figure 13. The resulting composite material consists of conductive networks throughout the specimen, which in turn, allows the composite material to display a high level of conductivity. Compared to a compression mold of the same material, the SLS printed component displayed higher levels of conductivity due to aligned channels. Further, the carbon black benefits the adsorption of laser energy due to its higher thermal conductivity than the polyamide 12. This work highlights a novel approach to creating materials that can be later printed with SLS 3D printing, hurdling the obstacle of limited material selection.[93]

Sha et al. devised an automated powder-bed printing method for *in situ* growth of 3D graphene foam by manually feeding layers of nickel and sucrose powder and sintering with a CO_2 laser. Sucrose served as the carbonaceous solid source for graphene, while the sintered Ni metal functioned as both the catalyst and template for the growth of graphene, and no high-temperature furnace or tedious growth process was required. The entire process can be seen in Figure 14. The product was largely porous (~99.3%), which brought the density down to approximately 0.015 g cm^{-3}. Moreover, the graphene foam had a remarkable storage modulus as well as a high room-temperature damping capacity when compared to other porous graphene foams. This simple and efficient method shows promising applications in fields requiring sound absorption, damping materials, and energy storage devices. [94]

Zhu et al. reported a route to fabricate green parts consisting of carbon fiber/SiC composites by incorporation of SLS and liquid silicon infiltration methods, which is the first time to use phenolic resin-coated carbon nanofibers as precursor powder. [95] In this study, the pores ranging from 15 to 30 μm were created from intercrossed carbon fibers in the first step of forming the powder and then the green parts composed of powder were made by advanced SLS to produce the voids with a diameter of 1.5 mm in lattice structures, which can be clearly observed in Figure 15. Subsequently, carbon nanofibers/carbon preform has been prepared by vacuum infiltration and subsequent carbonization. The resulting product of carbon fiber/SiC was synthesized by a second infiltration of liquid silicon. The physical properties were investigated at different laser power applied in SLS process, which showed the higher applied power would cause a lower average pore diameter. Other mechanical properties were also discussed, including density, flexural strength, and fracture toughness, which presented that the mechanical performance can be improved in part by integration of carbon fibers.

Lahtinen and his team of researchers[96] skillfully harnessed the capabilities of selective laser sintering (SLS) 3D printing to meticulously fabricate highly porous carbonous electrodes. Graphite powder was mixed into either polyamide-12, polystyrene, or polyurethane matrix for the purpose of

fabricating highly porous carbonous electrodes through the utilization of SLS 3D printing. Utilizing the innovative Selective Laser Sintering (SLS) printing technique, all the 3D printed electrodes exhibited exceptional porosity. Harnessing polyurethane as a pliable supporting matrix, researchers successfully engineered flexible electrodes. Remarkably, these electrodes demonstrated heightened sensitivity to both pressure and mechanical stress. The findings, derived from this study, elucidate that the synergistic combination of meticulous chemical design, intricate printing material, and the judicious application of SLS 3D printing, enable the fabrication of highly customizable, precision electrodes, boasting desirable chemical, physical, mechanical, and flow-through properties, tailored to meet specific functional requirements.

Selective laser sintering is a representative direct writing method.[97] Luo et al.[98] reported a facile and scalable direct laser writing (DLW)-assisted technique for generating porous carbon platelets (PCPs) with uniform size and arbitrarily designed shapes. This innovative approach leverages CO_2 laser irradiation to induce carbonization of a biomass composite sheet. This sheet is formed by infusing sodium lignosulfonate into cellulose paper, thereby creating porous carbon features of arbitrary design. Subsequent water immersion treatment facilitates the spontaneous detachment of the laser-written carbon features, resulting in freestanding PCPs. The fabrication, characterization, and potential applications of PCPs in diverse shapes were explored. These applications span dye adsorption, flexible sensors, and miniaturized supercapacitors.

Although powder bed fusion has been around for years, its application in producing porous carbon is still relatively new. As a result, few materials have been shown to produce porous carbon even for the most promising subcategory, SLS. Nevertheless, this route is advantageous since it produces relatively high carbon yield.[91] Furthermore, this process can utilize waste products as the carbon source, making it sustainable and inexpensive. Currently, most SLS research on porous carbon tends to look at preparation and characterization.[99–101] Thus, the potential of SLS technology for versatile applications could be further explored. Further research into material selection and synthesis looks at finding composites with desirable powder characteristics, thermal properties,[102] and material compatibility,[103] which promises to further enhance this process and expand the potential applications.

4. Conclusions and Perspectives

In recent years, the fusion of additive manufacturing with traditional methods has emerged as a promising intersection in the development of porous carbon materials for a wide range of applications, delivering cost-effectiveness, control, and repeatability. This hybrid approach has enabled the customization of both the macrostructure and microstructure of porous carbon, significantly enhancing material efficiency and optimization for specific applications.

Highlighting the technological strides in material fabrication, the integration of Artificial Intelligence (AI) and 3D printing technology has been particularly transformative. This is because AI can potentially predict properties, optimize synthesis processes, and enable high-throughput material screening for porous carbon, minimizing time and bandwidth for research and development. This synergy between AI and 3D printing is expected to greatly benefit porous carbon fabrication and its integration into various high impact sectors. Building on these integrations, the application of Machine Learning (ML) in 3D printing can enhance material selection, drives design innovation, and optimizes fabrication processes. By leveraging vast databases to pinpoint materials and process parameters with optimal properties, synthesis is can be more controlled with less overall waste. These improvements will not only streamline workflow, but also create avenues for more sustainability and cost-effectiveness.

Within the scope of 3D printing techniques—namely, material extrusion, vat polymerization, and powder bed fusion—the exploration of porous carbon fabrication has unveiled notable benefits and challenges. The adaptability of these techniques allows for the creation of porous carbon with tailored macrostructures and microstructures, offering promising opportunities across various sectors that require specific material architectures. Other aspects, including tailoring printing process precursors for controlled porosity, adding high-performance materials, and refining manufacturing parameters are also pivotal areas for further exploration. These advancements, coupled with the utilization of AI and ML, hold the potential to surpass existing limitations and provide great opportunities for manufacturing porous carbon and other materials with unparalleled precision and customization.

Author Contributions

All authors evaluated the review and approved the final version of the manuscript.

Conflicts of interest

There are no conflicts to declare.

Acknowledgements

References

1 S. Wang, D. Chen, Z. X. Zhang, Y. Hu and H. Quan, *Sep Purif Technol*, , DOI:10.1016/j.seppur.2022.120912.

2   H. Guan, Q. Wang, X. Wu, J. Pang, Z. Jiang, G. Chen, C. Dong, L. Wang and C. Gong, *Compos B Eng*, 2021, 207.

3   M. Avhad, V. Flaud, L. Burel, J. Cavailles, T. Sakpal, L. Lefferts and H. Kaper, *Carbon N Y*, 2020, **169**, 297–306.

4   L. Wang and X. Hu, *Chem Asian J*, 2018, 13, 1518–1529.

5   Q. Y. Zhou, L. Tan, T. B. Lv, M. C. Li, J. J. Zhang, Z. Q. Zhao, X. J. Jin, Z. Liu, P. P. Hou, Z. Zeng, S. Deng and G. P. Dai, *ACS Appl Mater Interfaces*, , DOI:10.1021/acsami.2c19987.

6   M. C. Li, Z. Liu, L. Tan, Q. Y. Zhou, J. J. Zhang, P. P. Hou, X. J. Jin, T. B. Lv, Z. Q. Zhao, Z. Zeng, S. Deng and G. P. Dai, *ACS Sustain Chem Eng*, 2022, **10**, 10223–10233.

7   W. Tian, H. Zhang, X. Duan, H. Sun, G. Shao and S. Wang, *Adv Funct Mater*, 2020, 30.

8   K. J. Chen, D. G. Madden, T. Pham, K. A. Forrest, A. Kumar, Q. Y. Yang, W. Xue, B. Space, J. J. Perry, J. P. Zhang, X. M. Chen and M. J. Zaworotko, *Angewandte Chemie - International Edition*, 2016, **55**, 10268–10272.

9   P. Hang, H. Hu and S. Dai, *Porous Carbon Supports:Recent Advances with Various Morphologies and Compositions*, 2015, vol. 7.

10   M. Ben Mosbah, L. Mechi, R. Khiari and Y. Moussaoui, *Processes*, 2020, 8, 1–24.

11   C. Vix-Guterl, E. Frackowiak, K. Jurewicz, M. Friebe, J. Parmentier and F. Béguin, *Carbon N Y*, 2005, **43**, 1293–1302.

12   S. Dutta, A. Bhaumik and K. C. W. Wu, *Energy Environ Sci*, 2014, 7, 3574–3592.

13   H. Zhang, Y. Zhu, Q. Liu and X. Li, *Appl Energy*, , DOI:10.1016/j.apenergy.2021.118131.

14   W. Kai, Z. Shengzhe, Z. Yanting, R. Jun, L. Liwei and L. Yong, *Int J Electrochem Sci*, 2018, **13**, 10766–10773.

15   Y. Wang, J. Chen, H. Ihara, M. Guan and H. Qiu, *TrAC - Trends in Analytical Chemistry*, 2021, 143.

16   M. S. Khosrowshahi, H. Mashhadimoslem, H. Shayesteh, G. Singh, E. Khakpour, X. Guan, M. Rahimi, F. Maleki, P. Kumar and A. Vinu, *Advanced Science*, 2023, 10.

17   A. K. Mohammed, S. Usgaonkar, F. Kanheerampockil, S. Karak, A. Halder, M. Tharkar, M. Addicoat, T. G. Ajithkumar and R. Banerjee, *J Am Chem Soc*, 2020, **142**, 8252–8261.

18   J. Fonseca and T. Gong, *Coord Chem Rev*, 2022, 462.

19   X. Yang, T. Lv and J. Qiu, *Small*, 2023, 19.

20   Y. Lu, S. Zeng, L. Zhou, X. Huang, Y. Zeng, D. Zheng, W. Xu and X. Lu, *Particle and Particle Systems Characterization*, , DOI:10.1002/ppsc.201900115.

21   Y. Zheng, X. Huang, J. Chen, K. Wu, J. Wang and X. Zhang, *Materials*, , DOI:10.3390/ma14143911.

22   W. Zong, N. Chui, Z. Tian, Y. Li, C. Yang, D. Rao, W. Wang, J. Huang, J. Wang, F. Lai and T. Liu, *Advanced Science*, , DOI:10.1002/advs.202004142.

23   W. Tian, H. Zhang, X. Duan, H. Sun, G. Shao and S. Wang, *Adv Funct Mater*, 2020, 30.

24   A. Memetova, I. Tyagi, R. R. Karri, V. Kumar, K. Tyagi, Suhas, N. Memetov, A. Zelenin, T. Pasko, A. Gerasimova, D. Tarov, M. H. Dehghani and K. Singh, *Chemical Engineering Journal*, 2022, 446.

25   Q. Zhang, B. Yan, L. Feng, J. Zheng, B. You, J. Chen, X. Zhao, C. Zhang, S. Jiang and S. He, *Nanoscale*, 2022, 14, 8216–8244.

26   J. Yin, W. Zhang, N. A. Alhebshi, N. Salah and H. N. Alshareef, *Small Methods*, 2020, 4.

27   M. A. Mudassir, S. Kousar, M. Ehsan, M. Usama, U. Sattar, M. Aleem, I. Naheed, O. Bin Saeed, M. Ahmad, H. F. Akbar, M. A. Ud Din, T. M. Ansari, H. Zhang and I. Hussain, *Renewable and Sustainable Energy Reviews*, 2023, 185.

28   B. A. Praveena, N. Lokesh, A. Buradi, N. Santhosh, B. L. Praveena and R. Vignesh, in *Materials Today: Proceedings*, Elsevier Ltd, 2022, vol. 52, pp. 1309–1313.

29   A. Jadhav and V. S. Jadhav, *Mater Today Proc*, 2022, **62**, 2094–2099.

30   I. Karakurt and L. Lin, *Curr Opin Chem Eng*, 2020, 28, 134–143.

31   M. P. Browne, E. Redondo and M. Pumera, *Chem Rev*, 2020, **120**, 2783–2810.

32   L. Y. Zhou, J. Fu and Y. He, *Adv Funct Mater*, 2020, 30.

33   P. Blyweert, V. Nicolas, J. Macutkevic, V. Fierro and A. Celzard, *ACS Sustain Chem Eng*, 2022, **10**, 7702–7711.

34   S. Saleh Alghamdi, S. John, N. Roy Choudhury and N. K. Dutta, , DOI:10.3390/polym13.

35   A. Osman and J. Lu, *Materials Science and Engineering R: Reports*, 2023, 154.

36   Q. Ge, Z. Li, Z. Wang, K. Kowsari, W. Zhang, X. He, J. Zhou and N. X. Fang, *International Journal of Extreme Manufacturing*, 2020, 2.

37   Y. G. Park, I. Yun, W. G. Chung, W. Park, D. H. Lee and J. U. Park, *Advanced Science*, 2022, 9.

38   R. Y. Tay, Y. Song, D. R. Yao and W. Gao, *Materials Today*, 2023, 71, 135–151.

39   D. Thomas, *International Journal of Advanced Manufacturing Technology*, 2016, **85**, 1857–1876.

40   A. P. Moreno Madrid, S. M. Vrech, M. A. Sanchez and A. P. Rodriguez, *Materials Science and Engineering C*, 2019, 100, 631–644.

41   J. A. Lewis, *Adv Funct Mater*, 2006, **16**, 2193–2204.

42   M. Schmid, A. Amado and K. Wegener, *J Mater Res*, 2014, **29**, 1824–1832.

43   H. Quan, T. Zhang, H. Xu, S. Luo, J. Nie and X. Zhu, *Bioact Mater*, 2020, 5, 110–115.

44   J. Shah, B. Snider, T. Clarke, S. Kozutsky, M. Lacki and A. Hosseini, *International Journal of Advanced Manufacturing Technology*, 2019, **104**, 3679–3693.

45   N. Shahrubudin, T. C. Lee and R. Ramlan, in *Procedia Manufacturing*, Elsevier B.V., 2019, vol. 35, pp. 1286–1296.

46   M. Spoerk, C. Holzer and J. Gonzalez-Gutierrez, *J Appl Polym Sci*, 2020, 137.

47   A. Y. Davis, Q. Zhang, J. P. S. Wong, R. J. Weber and M. S. Black, *Build Environ*, , DOI:10.1016/j.buildenv.2019.106209.

48   G. H. Loh, E. Pei, J. Gonzalez-Gutierrez and M. Monzón, *Applied Sciences (Switzerland)*, 2020, 10.

49   A. K. Gupta, Krishnanand and M. Taufik, in *Materials Today: Proceedings*, Elsevier Ltd, 2021, vol. 50, pp. 1234–1242.

50   S. J. He, K. Q. Zhang, Y. J. Zou and Z. H. Tian, *Xinxing Tan Cailiao/New Carbon Materials*, 2022, **37**, 898–917.

51   L. L. Jiao and J. H. Sun, in *Procedia Engineering*, Elsevier Ltd, 2014, vol. 71, pp. 622–628.

52   J. J. Schwartz, *MRS Bull*, 2022, 47, 628–641.

53   M. Pagac, J. Hajnys, Q. P. Ma, L. Jancar, J. Jansa, P. Stefek and J. Mesicek, *Polymers (Basel)*, 2021, 13, 1–20.

54   W. Li, L. S. Mille, J. A. Robledo, T. Uribe, V. Huerta and Y. S. Zhang, *Adv Healthc Mater*, 2020, 9.

55   G. González, D. Baruffaldi, C. Martinengo, A. Angelini, A. Chiappone, I. Roppolo, C. F. Pirri and F. Frascella, *Nanomaterials*, 2020, **10**, 1–13.

56   W. Piedra-Cascón, V. R. Krishnamurthy, W. Att and M. Revilla-León, *J Dent*, 2021, 109.

57   K. L. Sampson, B. Deore, A. Go, M. A. Nayak, A. Orth, M. Gallerneault, P. R. L. Malenfant and C. Paquet, *ACS Appl Polym Mater*, 2021, 3, 4304–4324.

58   W. L. Ng, J. M. Lee, M. Zhou, Y. W. Chen, K. X. A. Lee, W. Y. Yeong and Y. F. Shen, *Biofabrication*, 2020, 12.

59   Y. Zhang, Z. Dong, C. Li, H. Du, N. X. Fang, L. Wu and Y. Song, *Nat Commun*, , DOI:10.1038/s41467-020-18518-1.

60   D. Dev Singh, T. Mahender and A. Raji Reddy, in *Materials Today: Proceedings*, Elsevier Ltd, 2021, vol. 46, pp. 350–355.

61   S. Sun, M. Brandt and M. Easton, in *Laser Additive Manufacturing: Materials, Design, Technologies, and Applications*, Elsevier Inc., 2017, pp. 55–77.

62   A. Awad, F. Fina, A. Goyanes, S. Gaisford and A. W. Basit, *Int J Pharm*, , DOI:10.1016/j.ijpharm.2020.119594.

63   F. Bosio, A. Aversa, M. Lorusso, S. Marola, D. Gianoglio, L. Battezzati, P. Fino, D. Manfredi and M. Lombardi, *Mater Des*, , DOI:10.1016/j.matdes.2019.107949.

64   R. Singh, A. Gupta, O. Tripathi, S. Srivastava, B. Singh, A. Awasthi, S. K. Rajput, P. Sonia, P. Singhal and K. K. Saxena, in *Materials Today: Proceedings*, Elsevier Ltd, 2019, vol. 26, pp. 3058–3070.

65   M. Launhardt, A. Wörz, A. Loderer, T. Laumer, D. Drummer, T. Hausotte and M. Schmidt, *Polym Test*, 2016, **53**, 217–226.

66   A. Shahzad and I. Lazoglu, *Compos B Eng*, 2021, 225.

67   W. Zhang, H. Liu, X. Zhang, X. Li, G. Zhang and P. Cao, *Adv Funct Mater*, 2021, 31.

68   Z. Liu, X. Zhou and C. jun Liu, *Diam Relat Mater*, 2019, **95**, 121–126.

69   X. Zhou and C. jun Liu, *Catal Today*, 2020, **347**, 2–9.

70   L. Yang, X. Wang, S. Yin, X. Shi, L. Wang, P. She, Y. Song, Z. Liu and H. Sun, *Sep Purif Technol*, , DOI:10.1016/j.seppur.2023.124116.

71   B. Yao, H. Peng, H. Zhang, J. Kang, C. Zhu, G. Delgado, D. Byrne, S. Faulkner, M. Freyman, X. Lu, M. A. Worsley, J. Q. Lu and Y. Li, *Nano Lett*, 2021, **21**, 3731–3737.

72   Q. Li, Q. Dong, J. Wang, Z. Xue, J. Li, M. Yu, T. Zhang, Y. Wan and H. Sun, *J Power Sources*, , DOI:10.1016/j.jpowsour.2022.231810.

73   H. Jeong, J. H. Lee, S. Kim, S. Han, H. Moon, J. Y. Song and A. Y. Park, *Sci Rep*, , DOI:10.1038/s41598-023-47544-4.

74   K. Parate, S. V. Rangnekar, D. Jing, D. L. Mendivelso-Perez, S. Ding, E. B. Secor, E. A. Smith, J. M. Hostetter, M. C. Hersam and J. C. Claussen, *ACS Appl Mater Interfaces*, 2020, **12**, 8592–8603.

75   Z. Guo, P. Yu, Y. Liu and J. Zhao, *Compos Sci Technol*, , DOI:10.1016/j.compscitech.2020.108530.

76   S. S. Hossain and K. Lu, *Ceram Int*, 2023, 49, 10199–10212.

77   C. Oztan and V. Coverstone, *Acta Astronaut*, 2021, 180, 130–140.

78   M. L. Sesso, S. Slater, J. Thornton and G. V. Franks, *Journal of the American Ceramic Society*, 2021, **104**, 4977–4990.

79   H. Steldinger, A. Esposito, K. Brunnengräber, J. Gläsel and B. J. M. Etzold, *Advanced Science*, , DOI:10.1002/advs.201901340.

80   P. Wang, H. Zhang, H. Wang, D. Li, J. Xuan and L. Zhang, *Adv Mater Technol*, , DOI:10.1002/admt.201901030.

81   H. Jiang, S. Huang, H. Lv, D. Ge, X. He, P. Zhou, K. Xiao and Y. Zhang, *Water Res*, , DOI:10.1016/j.watres.2022.119134.

82   Y. Katsuyama, N. Haba, H. Kobayashi, K. Iwase, A. Kudo, I. Honma and R. B. Kaner, *Adv Funct Mater*, , DOI:10.1002/adfm.202201544.

83   A. Kudo, K. Kanamaru, J. Han, R. Tang, K. Kisu, T. Yoshii, S. ichi Orimo, H. Nishihara and M. Chen, *Small*, , DOI:10.1002/smll.202301525.

84   M. van der Heijden, M. Kroese, Z. Borneman and A. Forner-Cuenca, *Adv Mater Technol*, , DOI:10.1002/admt.202300611.

85   S. Chandrasekaran, J. B. Forien, P. G. Campbell, J. S. Oakdale, J. A. Mancini, M. A. Worsley and J. Biener, *Carbon N Y*, 2021, **179**, 125–132.

86   Q. Huang, S. Ni, M. Jiao, X. Zhong, G. Zhou and H. M. Cheng, *Small*, 2021, 17.

87   J. Martín-Montal, J. Pernas-Sánchez and D. Varas, *Polymers (Basel)*, , DOI:10.3390/polym13071147.

88   E. Johansson, O. Lidström, J. Johansson, O. Lyckfeldt and E. Adolfsson, *Materials*, , DOI:10.3390/ma10020138.

89   E. O. Olakanmi, R. F. Cochrane and K. W. Dalgarno, *Prog Mater Sci*, 2015, 74, 401–477.

90   P. J. Brown, *SELECTIVE LASER SINTERING (SLS) RAPID PROTYTPING TECHNOLOGY: A REVIEW OF MEDICAL APPLICATIONS*, .

91   K. A. Acord, A. D. Dupuy, U. Scipioni Bertoli, B. Zheng, W. C. West, Q. N. Chen, A. A. Shapiro and J. M. Schoenung, *J Mater Process Technol*, , DOI:10.1016/j.jmatprotec.2020.116827.

92   S. Guo, J. Li, L. Zhang and Y. Li, *Mater Lett*, , DOI:10.1016/j.matlet.2022.133300.

93   R. Hong, Z. Zhao, J. Leng, J. Wu and J. Zhang, *Compos B Eng*, , DOI:10.1016/j.compositesb.2019.107214.

94   J. Sha, Y. Li, R. Villegas Salvatierra, T. Wang, P. Dong, Y. Ji, S. K. Lee, C. Zhang, J. Zhang, R. H. Smith, P. M. Ajayan, J. Lou, N. Zhao and J. M. Tour, *ACS Nano*, 2017, **11**, 6860–6867.

95   W. Zhu, H. Fu, Z. Xu, R. Liu, P. Jiang, X. Shao, Y. Shi and C. Yan, *J Eur Ceram Soc*, 2018, **38**, 4604–4613.

96   E. Lahtinen, E. Kukkonen, J. Jokivartio, J. Parkkonen, J. Virkajärvi, L. Kivijärvi, M. Ahlskog and M. Haukka, *ACS Appl Energy Mater*, 2019, **2**, 1314–1318.

97   E. Hwang, J. Hong, J. Yoon and S. Hong, *Materials*, 2022, 15.

98   J. Luo, Y. Yao, M. Niu, X. Duan, R. Wang and T. Liu, *ACS Omega*, 2019, **4**, 5870–5878.

99   F. Yang, N. Zobeiry, R. Mamidala and X. Chen, *Mater Today Commun*, 2023, 34.

100   M. E. Korkmaz, M. K. Gupta, G. Robak, K. Moj, G. M. Krolczyk and M. Kuntoğlu, *J Manuf Process*, 2022, 81, 1040–1063.

101   F. E. Jabri, A. Ouballouch, L. Lasri and R. El Alaiji, *Journal of Achievements in Materials and Manufacturing Engineering*, 2023, 118, 5–17.

102   M. Schmid and K. Wegener, in *AIP Conference Proceedings*, American Institute of Physics Inc., 2016, vol. 1779.

103   A. Jandyal, I. Chaturvedi, I. Wazir, A. Raina and M. I. Ul Haq, *Sustainable Operations and Computers*, 2022, **3**, 33–42.
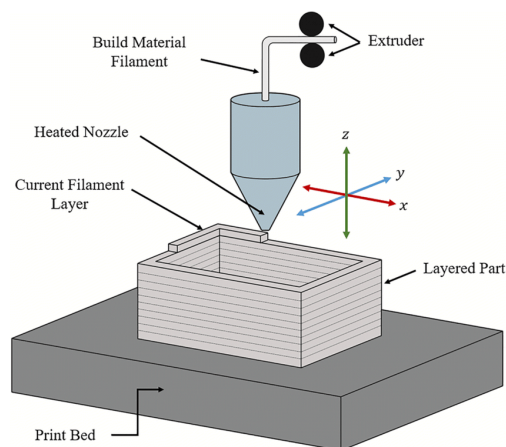
Figure 2: The basic working principle of material extrusion printing[44]

Figures to be placed accordingly:
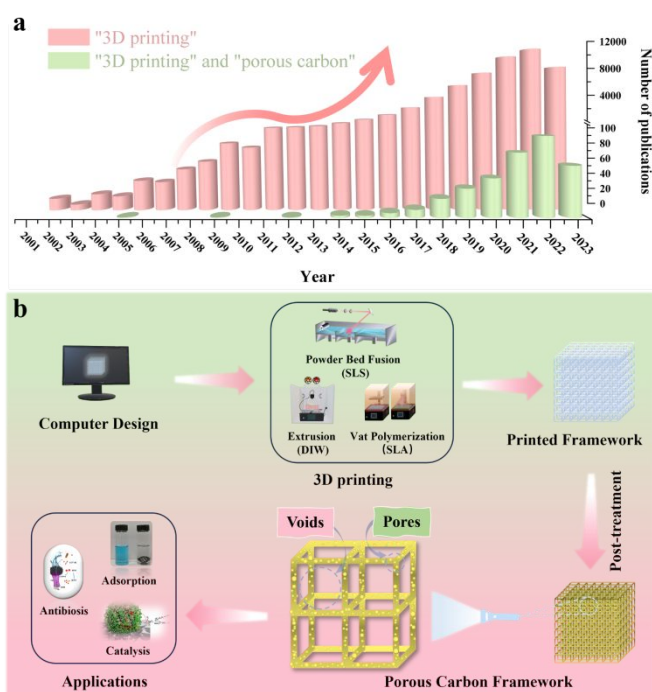
Figure 1: (a) The statistics of publications about "3D printing" and "porous carbon" since 2001 (Collected from Web of Science, Oct 2023); (b) a comprehensive illustration of the mechanistic relationship between computer design, 3D printing, and applications.
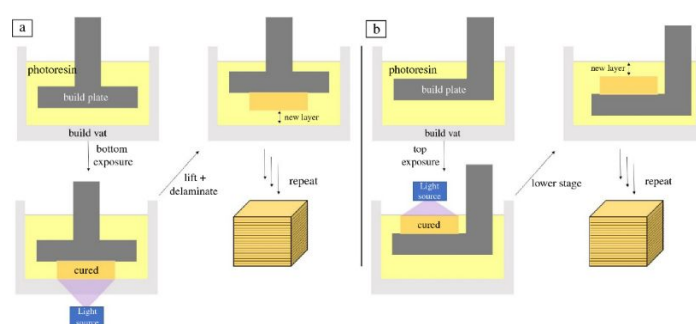
Figure 3: Schematic of layer-based vat photopolymerization where the light is oriented from the (a) bottom and (b) top[52]
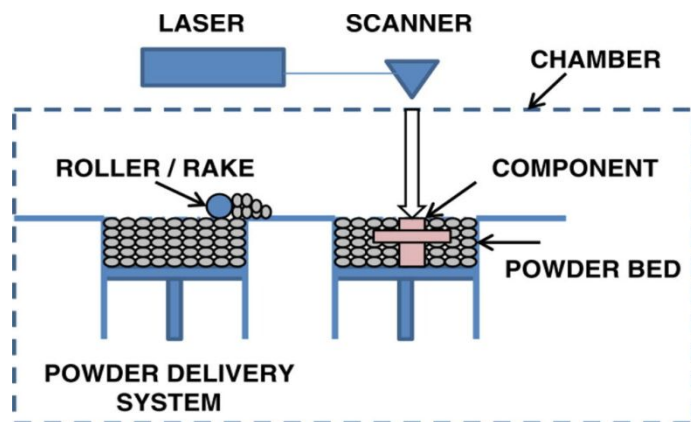
Figure 4: Schematic of Powder Bed Fusion[60]
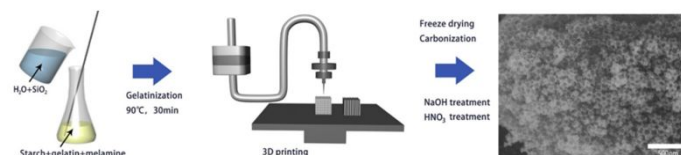
Figure 5: Schematic illustration of the DIW process to make porous carbon[68]
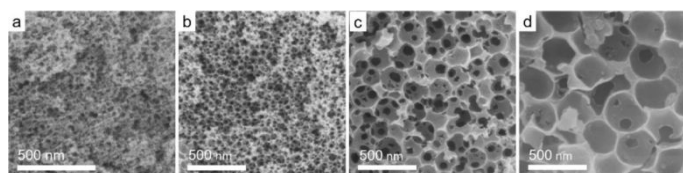
Figure 6: SEM of the printed carbon replicas with different SiO₂ diameters: (a) 50 nm; (b) 100 nm; (c) 200 nm; (d) 350 nm[69]
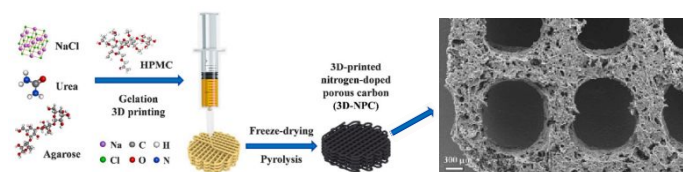
Figure 7: Schematic for the fabrication of 3D nitrogen-doped porous carbon by DIW and resulting morphology[70]
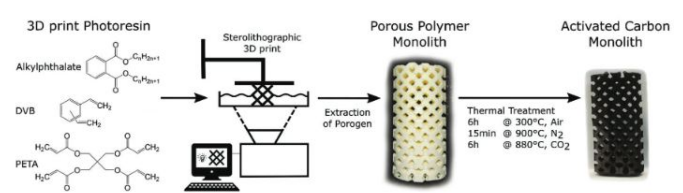

Figure 8: Schematic overview of the SLA printing process to create porous carbon[79]
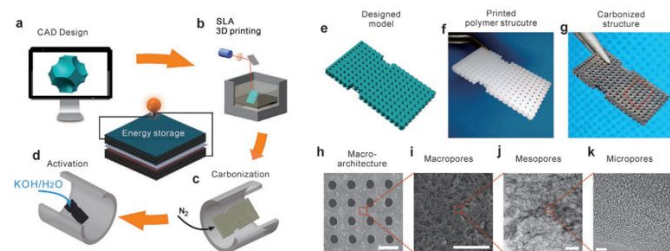
Figure 9: Schematic of the SLA print process and SEM/TEM imaging of macro-architecture, macropores, mesopores, and micropores with scale bars of 1 mm, 20 µm, 100 nm, and 5 nm, respectively[80]
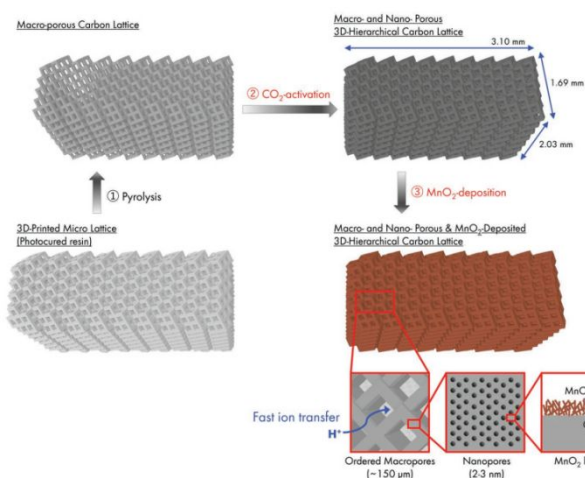
Figure 10: Schematic of process for the preparation of 3D-printed hierarchical porous carbon lattice with MnO₂ deposition[82]
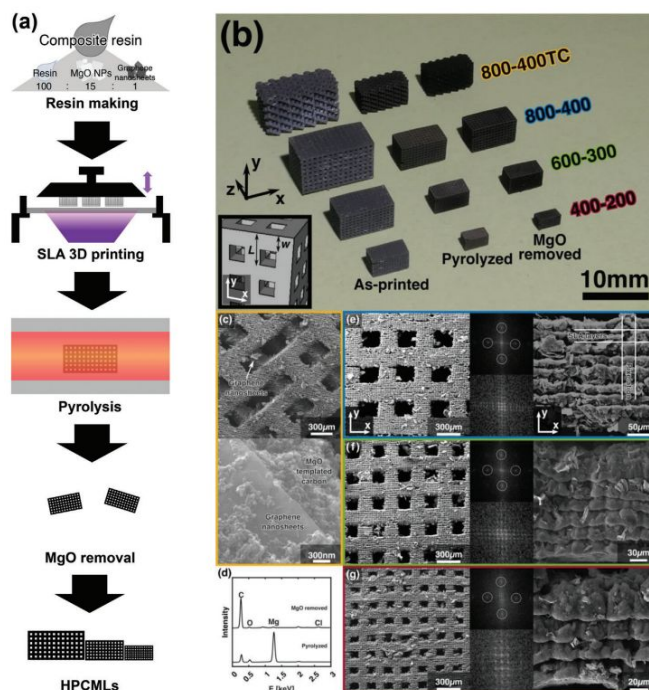

Figure 11: (a) schematic process for the preparation of hierarchical porous carbon microlattice by SLA; (b) An optical image of four types of samples at each step of preparation: as-printed, pyrolyzed, and MgO removed; (c) SEM images of sample 800-400TC with different magnifications; (e-g) SEM images with different magnifications and FFT patterns of the other three types of samples[83]
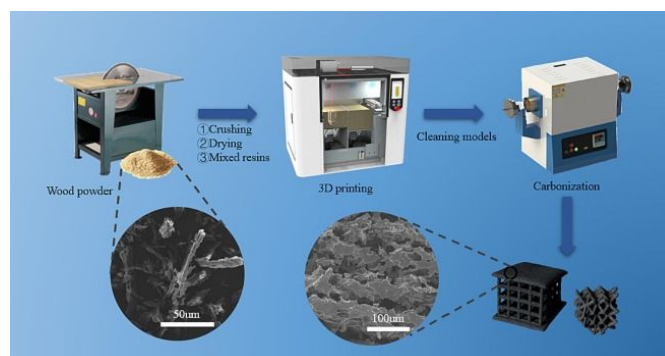

Figure 12: Schematic diagram of pine resin porous carbon electrode preparation by SLS[92]
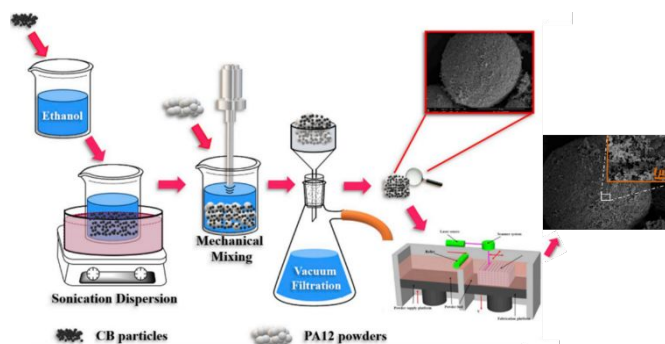
Figure 13: Schematic illustration of the two-step approach to making carbon black/polyamide 12 composites with 3D segregated conductive network.[93]
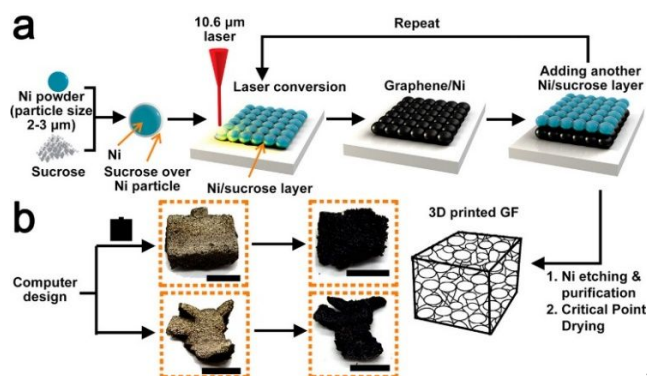
Figure 14: Schematic of in situ synthesis of 3D graphene foam using SLS[94]
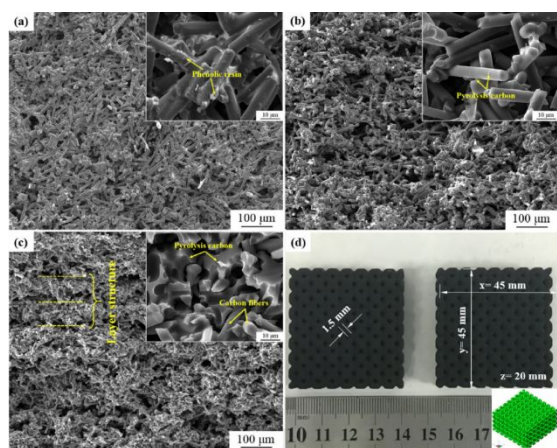
Figure 15: SEM images of (a) the SLS green part, cross-section of (b) the carbonized part and (c) the carbon fiber/C preform; (d) picture of complex green parts with lattice structures. The insets are the zoom-in SEM images.[95]

Table 1. Detailed comparison of different 3D printing technologies

Printing method	Resolution (Plane x-y)	Scalability (Base on supply chain)	Multi-material compatibility	Cost (Base on small batches)	Post-treatment	Advantages	Disadvantages	Ref.
Material Extrusion	Medium (1-100 μm)	Fair	Good (polymers with rheological properties)	Low (Inexpensive equipment and materials with abundant elections)	Required	Good multi-materials ability; Low-cost in small-scale printing	Low build speed; Post-curing	[32, 35, 38-39, 41]
Vat Polymerization	High (>600 nm)	poor	poor (photo-curable Polymers with low viscosity)	Medium (Cheap equipment, but relatively high cost starting materials)	Required	High resolution; Printable of complex structures with fine features	Supports needed; limitation of printing composite with high content; Post-curing	[32, 36, 40, 43]
Powder Bed Fusion	Low (>100 μm)	Good	Poor (Thermoplastic polymers powder)	High (High-cost materials and relatively expensive equipment)	Not required	Super high build speed; Support free	Low resolution; High processing temperature; High machine and materials cost for starters	[32, 37, 40, 42]

Table 1: Summary of 3D printing methods and their resolution, scalability, material compatibility, cost, advantages, disadvantages, and post process requirements